THE ASTROPHYSICAL JOURNAL, 346:983–990, 1989 November 15

H_2O MASERS IN STAR-FORMING REGIONS

MOSHE ELITZUR
University of Kentucky, Lexington
DAVID J. HOLLENBACH
NASA Ames Research Center
AND
CHRISTOPHER F. MCKEE
University of California, Berkeley
Received 1988 May 31; accepted 1989 May 22

ABSTRACT

We present a comprehensive model for the powerful H_2O masers observed in star-forming regions. In this model the masers occur behind shocks propagating in dense regions (preshock density is $\sim 10^7$ cm^{-3}). We present detailed numerical calculations, using the latest available data, of the shock structure and the maser pumping scheme, and show that the results can be summarized with some simple, yet powerful and accurate, scaling relations. The masers are velocity-coherent filamentary structures in the shocked material, pumped by excitations of the H_2O rotation states in collisions with neutrals. This paper focuses on high-velocity (≥ 50 km s^{-1}) dissociative shocks in which the heat of H_2 reformation on dust grains maintains a large column of ~ 400 K gas, where the chemistry drives a considerable fraction of the oxygen not in CO to form H_2O. The H_2O column densities produced by these shocks are sufficiently high to enable powerful maser action. A critical ingredient in determining the shock structure is the magnetic pressure, and the fields required by our model are in agreement with recent observations. The observed brightness temperatures (generally $\sim 10^{11}$–10^{14} K) are the result of filamentary aspect ratios (length/diameter) of ~ 5–50 in the postshock gas. Except for two exceptional burst events, our model is capable of explaining all the observed galactic H_2O masers—including the most luminous features in W49, the most powerful maser in the galaxy. We suggest that this model may account for the luminous extragalactic masers as well. According to this model, luminous masers may indicate the presence of enhanced magnetic fields. We also provide estimates for the anticipated luminosities in other H_2O maser transitions.

Subject headings: masers — magnetic fields — molecular processes — shock waves

I. INTRODUCTION

Although H_2O masers have long been recognized as prominent signposts of the star formation process, they remain a formidable challenge to theoretical understanding. The maser spots appear to be individual clumps, streaming away from some center of activity at velocities that can sometimes approach ~ 200 km s^{-1}. Individual features typically have apparent sizes of $\sim 10^{13}$ cm and brightness temperatures in the range $T_b \sim 10^{12}$–10^{13} K (Genzel 1986). Two cases of substantially higher brightness temperatures ($T_b > 10^{15}$ K) have been reported for flares, one in W49 (Burke *et al.* 1973) the other in Orion (Matveenko, Moran, and Genzel 1982). The isotropic luminosity of individual maser features ranges from less than 10^{-5} $L_\odot$ to 0.08 $L_\odot$ in the Galaxy (Walker, Matsakis, and Garcia-Barreto 1982); extragalactic masers have been observed with isotropic luminosities of up to 350 $L_\odot$ (Claussen, Heiligman, and Lo 1984).

Several properties of the maser features can be deduced directly from observations. The high brightness temperatures have led several investigators to suggest that the masers arise in filaments, which beam the radiation into a small angle (Goldreich and Keeley 1972; Genzel 1986; Matveenko 1986); in the case of W49, Genzel finds that the overall H_2O spectrum can be fitted by a collection of randomly oriented filaments with aspect ratios in the range of 3–20. Pumping by an external source of radiation is ruled out by observations (e.g., Genzel 1986) and an internal source of pump energy, such as produced in a shock, seems required. The development of powerful shocks in maser regions is inevitable in light of the high velocities observed in these sources.

Previous models for interstellar masers have invoked unusually high densities ($\gtrsim 10^9$ cm^{-3}) in the *preshock* gas. Strelnitskij (1980, 1984) and Kylafis and Norman (1986) have proposed an inversion mechanism which utilizes two kinds of particles (e.g., electrons and H_2 molecules) with different temperatures but comparable collision rates. Because of the assumed two-temperature plasma, this collisional mechanism can operate at high densities ($n \gtrsim 10^{11}$ cm^{-3}, where n is the hydrogen nuclei density) which would ordinarily thermalize the levels and quench the maser in a one-temperature plasma; therefore, the Strelnitskij mechanism can, in principle, produce arbitrarily high brightness temperatures. Kylafis and Norman suggest *C*-shocks (shocks with strong ambipolar diffusion; see Draine 1980) as a potential source of such high-density, two-temperature plasma. It remains to be demonstrated, however, that *C*-shocks could maintain a significant temperature difference between electrons and neutrals at these high densities. In the only detailed astrophysical scenario for water masers available to date, Tarter and Welch (1986) have recently proposed a shock model in which powerful ~ 100 km s^{-1} shocks radiatively pump extremely dense ($\sim 10^9$ cm^{-3}) preshock gas to produce the H_2O masers. We propose here a model with much less severe energy requirements; ~ 100 km s^{-1} shocks into $\sim 10^7$ cm^{-3} preshock gas, with the collisionally pumped H_2O

maser produced in the compressed, warm and accelerated postshock material.

Interstellar shocks provide a natural location for interstellar water masers: the energy to pump the maser is provided by the dissipation of the relative kinetic energies of the shocked and unshocked gas. The high temperatures in shocks lead to the production of copious amounts of H_2O (e.g., Elitzur 1979). Finally, shock fronts are by their very nature sheetlike, and regions in the shock plane which have coherent velocities will generally be elongated; i.e., filamentary. In principle, maser emission could arise in either C-shocks ($v_s \lesssim 40$–50 km s^{-1}; Chernoff, Hollenbach, and McKee 1982) or in J-shocks ($v_s \gtrsim 40$–50 km s^{-1}; negligible ambipolar diffusion). To date, detailed studies of the structure of interstellar shocks at the high densities characteristic of water masers have been carried out only for J-shocks (Hollenbach and McKee 1989; Elitzur, Hollenbach, and McKee 1989). These calculations show that J-shocks in dense clouds ($n_0 \sim 10^7$ cm^{-3}) develop a high-density ($n \sim 10^9$ cm^{-3}), high postshock temperature ($T \sim 400$ K) plateau, rich in H_2O. In such shocks the molecules are first completely dissociated by the extremely high postshock temperatures ($\sim 10^5$ K) immediately behind the shock front. Further downstream, where the material cools down, H_2 molecules reform on the dust grains, which can survive the shocks, and are ejected to the gas phase with sizable internal energies which provide a source of heating for the gas. The hydrogen column density of the heated region can be as large as $\sim 10^{22}$ cm^{-2} or greater, the H_2O column density as high as 3×10^{19} cm^{-2}, and the temperature is of order 400 K—warm enough to populate the maser levels which lie ~ 600 K above ground. This plateau therefore suggests itself as a natural site for H_2O maser action (Hollenbach, McKee, and Chernoff 1987).

In the model we propose, the pump mechanism in the postshock gas is the excitation of the H_2O to high rotational levels by collisions with H and H_2 molecules at $T \approx 300$–400 K. Consider the maser emission from a uniformly pumped, saturated maser with length l along the line of sight whose radiation is beamed into a solid angle Ω_m. If Φ_m is the volume production rate of maser photons, the brightness temperature can be obtained from (e.g., Elitzur 1982)

$$T_b = \frac{\lambda^2 h\nu \Phi_m l}{2k\,\Delta v \Omega_m}, \tag{1.1}$$

where λ is the wavelength and ν the frequency of the maser transition (1.35 cm and 22 GHz, respectively, for the H_2O maser line.) When the maser is shaped like a filament with an aspect ratio a (equal to length/diameter), $l \propto a$ and $\Omega_m \propto a^{-2}$. Thus, the brightness temperature along the axis of a saturated, collisionally pumped filamentary maser varies as a^3. For a filament of width $d = 10^{13} d_{13}$ cm and aspect ratio $a = 10 a_1$ the brightness temperature is

$$T_b = 1.34 \times 10^{11} \lambda^2 \eta_{-2} q_{-11} x_{-4}(H_2O) n_9^2 d_{13} \Delta v_5^{-1} a_1^3 f \text{ K}. \tag{1.2}$$

where $q = 10^{-11} q_{-11}$ cm^3 s^{-1} is the pump rate coefficient, $\eta = 10^{-2}\eta_{-2}$ is the fraction of these pumping events which produce a maser photon, $\Delta v = \Delta v_5$ km s^{-1} is the line width, $n_9 = n/10^9$ cm^{-3} and the H_2O density is $n(H_2O) = 10^{-4} x_{-4}(H_2O) n$. The factor f is the ratio of the solid angle of the filament cap as viewed from the other end to the maser beaming angle. In the Goldreich and Keeley (1972) cylindrical maser model, $f = 1$. A more detailed calculation shows that $f = 11/16$ (Elitzur, McKee, and Hollenbach 1989). We chose to display the dependence on f explicitly. Although the maser is pumped in a partially dissociated gas, we make the conservative assumption that the average pumping rate into the maser levels is the same as in a purely molecular gas, $\frac{1}{2} nn(H_2O) q$. It is important to note that the unrestricted increase of brightness temperature with source dimension displayed by equation (1.2) applies only to geometries such as slabs or cylinders where the IR-photons produced in the maser pump and loss transitions can leak out in a short distance sideways. In the case of a sphere, for example, the brightness temperature will not increase with source size beyond a certain radius at which the interior thermalizes.

The model we propose is therefore the following: The masers are located behind shocks that develop in star-forming regions. The shocks are the result of interaction of dense ($n_0 \sim 10^7$ cm^{-3}), high-velocity clumps (possibly embedded in the winds from young stellar objects) with dense ($\sim 10^6$–10^7 cm^{-3}) shells or clumps in the ambient medium. The shocked material is a thin slab in physical space, but breaks up into a network of filaments in velocity space. These filaments are the individual H_2O maser features. A single shock can give rise to many masers, although because of the small beaming angles none may be visible to a given observer.

In § II we present the results of maser model calculations. These are of general nature and provide the maximum brightness temperatures that can be produced in single-temperature environments of any kind. Section III describes the shock calculations which show that the parameters required for peak maser efficiency will be obtained behind J-shocks in star-forming regions. The implications of our model and connections with observations are discussed in § IV.

II. MASER EMISSION

We have performed detailed calculations of the H_2O level populations for a range of parameters that are likely to occur in star-forming regions. The populations of the 40 lowest levels of ortho–H_2O (all the levels with energies below 1260 cm^{-1}) were solved using the escape probability method and taking into account all the collisional and radiative processes that couple them. The calculations were performed using new cross sections, generously supplied by S. Green, for H_2O excitation in collisions with H_2 (Palma *et al.* 1988). These rates were computed utilizing the most recent advances in molecular potential theory, and are an improvement over the previously published rates (Green 1980). The rates for excitations by atomic hydrogen are at present more uncertain than the H_2–H_2O rates. We have tested the sensitivity of our results to the H_2 rates assumed and find that deviations from the nominal values can either raise or lower the pump efficiency, but that the basic inversion is robust. Charged particle collisions can be neglected because of their smaller rates. The proposal that inversion is due to collisions with charged and neutral particles held at different temperatures (Strelnitskij 1980) does not apply to J-shocks, where the electrons and neutrals have the same temperature.

These calculations are essentially identical to those performed by Cooke and Elitzur (1985) in their study of H_2O masers in late-type stars, with the improvement of the new cross sections and the inclusion of a larger number of levels (this was made possible by the larger set of cross sections available now). Apart from the obvious difference in the range of parameters covered in the two studies, the main change is in

the functional form of the escape probability. The Cooke and Elitzur investigation was concerned with an expanding wind and employed the appropriate large-velocity-gradient escape probability. In the present case, on the other hand, the appropriate geometry is that of a sheet of gas behind a shock. The velocity gradients for certain directions in the plane of the slab will be smaller than others. The better velocity coherence produces more favorable conditions for maser action, resulting in maser structures elongated in these directions (e.g., Alcock and Ross 1985). This leads to the formation of filamentary masers whose diameters are equal to the slab thickness d. However, the velocity gradients in the plane of the slab have no effect on photon escape of ordinary, nonmaser radiation, which occurs mostly in the perpendicular direction through the two faces of the slab. For these transitions, the present study therefore utilizes the escape probability of a quiescent slab with thickness d (Cappriotti 1965). Absorption by the dust of radiation generated in the pump cycle is neglected. This is a conservative approximation since including the effect can only increase the pump efficiency (Strelnitzkij 1978).

The maser effect was handled in the calculations in two different ways, corresponding to standard methods available in the literature. In the first approach, which is the one employed by Cooke and Elitzur among others, the maser radiation too is handled with the escape probability method. The relevant expression for maser escape probability was given by Elitzur (1982). In the present case the maser optical depth is calculated along the length of the filament ad and the escape probability is reduced by $\Omega/4\pi$ to account for the beaming of the radiation. Like the other levels, the population of the maser system obtained from the solution of the full set of coupled, nonlinear rate equations is then consistent with the effects of both the exchange processes and radiative transfer. The maser level populations obtained this way (and the maser optical depth) therefore properly account for the effect of saturation because it is incorporated into the solution of the rate equations themselves. The emissivity is then calculated utilizing the standard escape probability relation.

The other approach for handling the maser effect is based upon the fact that maser behavior in the saturated regime is fully determined by properties of the unsaturated solution (e.g., Elitzur 1982). The photon emission rate per unit volume during saturation, Φ_m, is determined by the rates for pumping into the two maser levels. These rates, which can be equivalently expressed in terms of an average pump rate q and an inversion efficiency η, reflect the interaction of the maser system with other levels in the pumping scheme and are independent of the saturation effect. The same holds true for the maser loss rate, which controls the transition to saturation. These quantities can therefore be calculated from a "pump model" which neglects the interaction with the maser radiation and then inserted as input parameters in a complete analytic two-level maser model, appropriate for the geometrical situation (Lucas 1980). This approach is justified because although saturation has a dramatic effect on the population difference of the maser levels, its impact on the level populations themselves is negligible. The change in populations of the two maser levels during the saturation process is minimal (Elitzur 1982), and the overall solution for the level populations is essentially the same with and without the inclusion of the maser radiative interaction. In the present case, the appropriate maser model is the cylindrical maser solution of Goldreich and Keeley (1972) with an allowance for a possibly different beaming angle; in the limit of $a \gg 1$, where the maser core can be neglected, the intensity obtained from this solution takes the form of equation (1.2).

We performed detailed numerical calculations using both techniques. The results obtained were essentially identical. The equivalence of these two methods can in fact be demonstrated rigorously (Elitzur 1989). We choose to present all of our results using the second approach where a numerical pump solution provides input parameters for the analytic cylindrical maser model. This method provides a simpler numerical framework and lends itself better for discussion because the dependence on various physical quantities is explicit.

Inversion of the H_2O 22 GHz line under saturated conditions and for reasonable aspect ratios was obtained for a wide range of densities ($\lesssim 10^{10}$ cm^{-3}) and temperatures ($\gtrsim 300$ K). The inversion is due to collisions with hydrogen, and is similar in nature to that obtained by Cooke and Elitzur. It occurs because levels on the "backbone" ladder (the lowest level for each J) are more strongly coupled (both collisionally and radiatively) than levels off the backbone. The backbone levels therefore establish among themselves a population distribution in thermal equilibrium while levels off the backbone are populated only by decays from higher backbone levels. This pattern leads to a number of inverted transitions, with the $6_{16} \rightarrow 5_{23}$ being the longest wavelength inversion. Similar results were first obtained by de Jong (1972), even though he had to rely on cross sections that were only a guess. Thus, the general properties of the solution do not depend on the exact values of the cross sections, although the details do.

We discovered that the results of the numerical calculations can be summarized quite accurately with some simple scaling relations. To understand the nature of the scaling variable, note that when all the line optical depths τ_{ij} are large, the escape probabilities for non-maser transitions become proportional to τ_{ij}^{-1} and the model parameters enter the rate equations of the pump model only in the combination $n\tau_{ij} \propto nn(H_2O)d/\Delta v$. The parameter

$$\xi \equiv x_{-4}(H_2O) n_9^2 d_{13}/\Delta v_5 , \tag{2.1}$$

effectively the maser emission measure, therefore suggests itself as a useful scaling variable. In terms of ξ, the saturated maser brightness temperature (eq. [1.2]) is

$$T_b = 1.34 \times 10^{11} \lambda^2 \xi \eta_{-2} q_{-11} a_1^3 f \text{ K} . \tag{2.2}$$

Our detailed calculations show that the numerical results are indeed similar for pump models with parameters in the range of interest, when compared at the same value of ξ. Since at large a the brightness temperature is proportional to $\xi\eta q$ (eq. [2.2]), and since both η and q turn out to be unique functions of ξ, *the run of T_b versus ξ for a fixed aspect ratio is model independent*, provided the maser saturates for the particular model and aspect ratio. The brightness temperature of the 22 GHz maser is plotted in Figure 1 as a function of ξ for $T = 400$ K and various aspect ratios, assuming $f = 1$. This figure provides a universal curve for a temperature of 400 K, as long as the densities do not exceed $\sim 10^{10}$ cm^{-3}. In particular, the peak brightness temperature $T_{b,\text{peak}}$ is obtained for $\xi \simeq 24$, for which we find $\eta_{-2} = 0.5$ and $q_{-11} = 0.5$, so that

$$T_{b,\text{peak}} \simeq 1.5 \times 10^{12} a_1^3 f \text{ K} . \tag{2.3}$$

The brightness temperature decreases slowly with ξ away from the peak; a full order of magnitude decrease in ξ, from 24 to

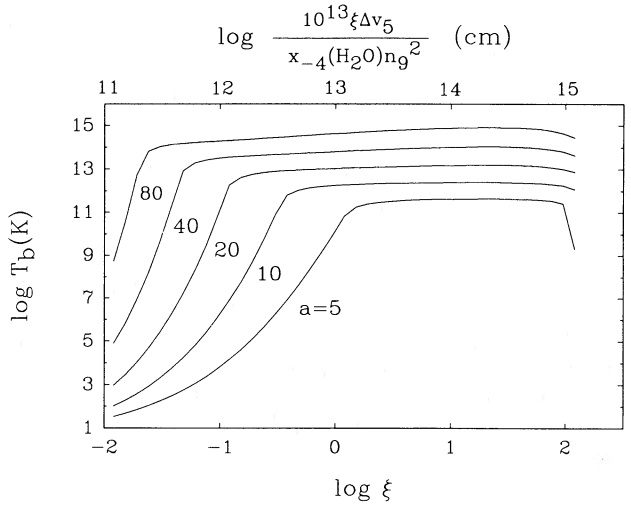

FIG. 1.—Brightness temperature of filamentary H_2O 22 GHz masers as function of the dimensionless parameter ξ (see text) at $T = 400$ K for various aspect ratios a, as marked on the curves. The top axis provides the corresponding filamentary diameter d, which depends on n, $x(H_2O)$, and Δv.

2.4, leads to a drop of only $\sim 50\%$ in T_b. When ξ decreases further to 0.24, T_b declines by an additional factor of ~ 3, provided the aspect ratio is large enough that the maser remains saturated ($a \geq 10$). For $\xi > 24$ the decline in T_b is again moderate until the abrupt falloff when ξ exceeds 120 and the maser is quenched. We note that because of the large column densities, radiative decays are slowed down by photon trapping and the immediate loss mechanism of the maser system is in fact due to collisions. Still the inversion does not quench until higher densities because of the small energy separation of the maser levels which allows inversion for rather small differences in the pump rates. This point will be discussed at greater detail in a subsequent paper (Elitzur, Hollenbach, and McKee 1989).

The top axis of Figure 1 displays the quantity $\{\xi \Delta v_5/[x_{-4}(H_2O)n_9^2]\} \times 10^{13}$ cm, the diameter d corresponding to ξ for given model parameters. Typically, the factor in curly brackets is ~ 1–10 in masing shocks, as we show below, and the expected maser diameters are $\sim 10^{13}$–10^{14} cm, in agreement with observations. At large d (whose precise value depends on the parameters of the filament) the inversion is quenched. The maser levels thermalize because of radiative trapping in the transitions that connect them to other levels. The effect of dust on the radiative transfer, which was neglected here, could conceivably allow larger diameters. Maser features with bigger sizes correspond to filamentary models with lower densities which thermalize at larger diameters (note that $d \propto n^{-2}$ when ξ is fixed.)

Another quantity directly related to observations is the isotropic maser luminosity $L_m = (2\pi^2/\lambda^3)kT_b d^2 \Delta v$. Combining this with equation (2.2) yields

$$L_m = 9.36 \times 10^{-7} \lambda^{-1} \xi \eta_{-2} q_{-11} a_1^3 d_{13}^2 \Delta v_5 f L_\odot \quad (2.4)$$

so that for a 22 GHz maser operating near its peak brightness temperature,

$$L_m = 4.2 \times 10^{-6} a_1^3 d_{13}^2 \Delta v_5 f L_\odot . \quad (2.5)$$

The numerical calculations also show that for the same ξ, the maser intensity is approximately proportional to the temperature (η is essentially T-independent while $q \propto T$ in the temperature range $\sim$300–800 K). Thus, if the temperature is raised to 600 K, T_b and L_m both increase by $\sim 50\%$.

III. SHOCK STRUCTURE

Dense dissociative shocks can produce the masing filaments described in § II. A numerical code for such shocks has been developed by Hollenbach and McKee (1979) (hereafter HM; see also Hollenbach McKee, and Chernoff 1987, and Hollenbach and McKee 1989). It follows the ionization, recombination, thermal balance, and chemistry behind J-type shocks with speeds $v_s \lesssim 300$ km s^{-1} and preshock densities $n_0 \lesssim 10^8$ cm^{-3}. Because H_2O masers are observed with velocities ranging from 0 to 300 km s^{-1}, we take 100 km s^{-1} as a typical shock velocity. Our results are relatively insensitive to the shock velocity *as long as the shocks completely dissociate* H_2 ($v_s \gtrsim 40$–50 km s^{-1}). The density in the masing region in the shock is limited by the magnetic field to

$$n = 7.7 \times 10^8 (n_{07} v_{s7}/b) \text{ cm}^{-3} , \quad (3.1)$$

where $n_{07} = n_0/10^7$ cm^{-3}, $v_{s7} = v_s/100$ km s^{-1}, and b provides the component of the preshock magnetic field perpendicular to v_s by the relation $B_{0\perp} = bn_0^{1/2}$ μG with n_0 in cm^{-3} (see HM); in terms of b, the Alfvén velocity ahead of the shock is $1.84b$ km s^{-1}. Since the inferred densities in masers are of order 10^9 cm^{-3}, we adopt $n_0 \sim 10^7$ cm^{-3} as a typical preshock density.

Immediately behind the shock front the gas temperature is of order 10^5 K, and the gas species become completely dissociated and almost entirely ionized. At a hydrogen nucleus column density $N \approx 10^{18}$ cm^{-2} downstream from the shock front, the gas has cooled to $\sim 10^4$ K and the ions recombine. Further downstream, the gas cools to a temperature ($\lesssim$3000 K) where H_2 collisional dissociation is negligible and H_2 begins to reform on grain surfaces. Grains survive these 100 km s^{-1} shocks; the results of McKee *et al.* (1987) indicate that less than $\sim 40\%$ of the mass of silicate grains will be vaporized in 100 km s^{-1} shocks. The grains are not well coupled to the gas temperature at these postshock densities ($n \sim 10^9$ cm^{-3}) and gas temperatures ($T \sim 10^3$ K), so their temperatures are typically $T_{gr} \sim 100$ K. Hydrogen molecule formation on their surfaces at these elevated grain temperatures is somewhat problematic, but likely if the grain surfaces include sites of enhanced binding for H atoms (see HM).

Figure 2 is the result of the shock code for $n_0 = 10^7$ cm^{-3}, $v_s = 100$ km s^{-1}, and $b = 0.5$ (corresponding to $B_{0\perp} = 1.5$ mG in the preshock gas). The ratio of impurity or defect sites (sites which bind H atoms tightly) to the physically absorbing sites on grains is taken to be 0.03. This ratio is important in calculating γ, the rate coefficient for H_2 formation on grains, when $T_{gr} \gtrsim 100$ K, as is the case in shocks with $n_{07} v_{s7}^3 \gtrsim 1$ (see HM). Figure 2 graphically shows the portion of the postshock structure relevant to H_2O maser production—the temperature region between 3×10^3 K and 100 K where molecules are reformed and where collisional excitation of the high-lying maser transition is efficient. It shows the conversion of nearly all oxygen not tied up in CO to H_2O, so that $x_{-4}(H_2O) \sim 2$. The value of ξ for gas at $T \geq 300$ K is given by $\xi_{\text{shock}} = 7.1$ in this case.

The main feature of interest is the temperature plateau at $\sim T = 400$ K. The heating mechanism which causes this plateau is the deposition of the heat of H_2 formation into the gas thermal reservoir. H_2 forms on grain surfaces and is ejected

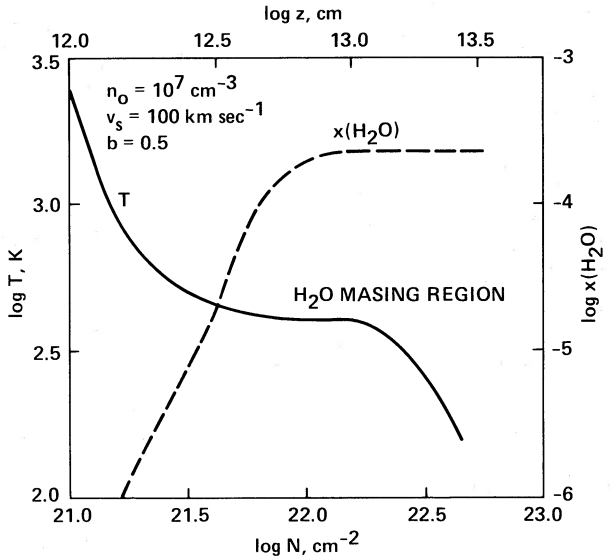

FIG. 2.—The temperature and water abundance profiles behind a 100 km s^{-1} shock incident upon a gas of hydrogen nuclei density $n_0 = 10^7$ cm^{-3} and magnetic field component $B_{0\perp} = 1.5$ mG perpendicular to the shock velocity vector. N is the H-nuclei column density, and z is the distance, both measured from the shock front, and $x(H_2O)$ is the abundance of H_2O relative to hydrogen. The H_2O maser is collisionally pumped in the high H_2O abundance region near $T \sim 300$–500 K, a region heated by the formation energy of H_2. The postshock density at this point, given in eq. (3.1), is 1.5×10^9 cm^{-3}. The value of ξ produced by this shock is 7.1.

into the gas with ~ 4 eV of vibrational and rotational energy.[1] At low densities this energy is radiated away by infrared quadrupole transitions, but at densities greater than the critical density ($\sim 10^5$ cm^{-3} for collisions with H atoms and $\sim 10^8$–10^9 cm^{-3} for collisions with H_2 at 500 K), the energy is collisionally transferred to gas heating. This heating persists until all the atomic hydrogen is converted to H_2, corresponding to a postshock column density $N_f \simeq n_0 v_s t_{H_2}$, where t_{H_2} is the formation time for H_2. Assuming that the post-shock compression is limited by the magnetic field, we obtain for the column N_{plat} of the temperature plateau

$$N_{plat} \simeq N_f \simeq 1.3 \times 10^{22} b/\gamma_{-17} \text{ cm}^{-2} , \quad (3.2)$$

where $\gamma = 10^{-17}\gamma_{-17}$ cm^3 s^{-1}.

The temperature T_{plat} of this plateau can be estimated by equating the H_2 formation heating to the dominant H_2O cooling using the analytic cooling formula of HM in the optically thick limit with $\eta_{JT} = 175 T_3^{3/2}$ in order to fit the numerical results of Neufeld and Melnick (1987):

$$T_{plat} \simeq 400(n_{07} v_{s7}/\Delta v_5)^{2/9} \text{ K} . \quad (3.3)$$

This temperatue is quite robust for $n_0 \gtrsim 10^5$ cm^{-3}; the insensitivity to b and γ arises because both the heating and cooling mechanisms have identical dependences on these parameters.

[1] Reliable laboratory confirmation of this theoretical prediction (Hollenbach and Salpeter 1971; Hunter and Watson 1978; Duley and Williams 1986) is not available, but generally supportive (see Lin and Somorjai 1985; Comsa and David 1985). Shutte *et al.* (1976) review previous work and perform the most relevant laboratory experiment; their conclusion is that roughly one-half of the recombination energy is ejected into the gas when the surface coverage of adsorbed H_2 is small (as will be the case for the warm grains behind these shocks.) However, uncertainties in the recombining fraction could raise this estimate.

T_{plat} is also independent of the H_2O abundance as long as cooling is suppressed by large optical depths. The temperature plateau quickly disappears for preshock densities below $\sim 10^5$ cm^{-3} because of less efficient collisional de-excitation of H_2.

We identify the width d of the maser spot with the thickness of the post shock maser layer, or

$$d = N_{plat}/n \simeq 1.3 \times 10^{13} \frac{b}{\gamma_{-17} n_9} \text{ cm}$$

$$= 1.7 \times 10^{13} \frac{b^2}{\gamma_{-17} n_{07} v_{s7}} \text{ cm} . \quad (3.4)$$

This compares favorably with the observed maser spot size (see Genzel 1986) if the various parameters are of order unity.

As discussed in § II, conditions conducive to bright maser emission are produced when $T \gtrsim 300$ K, $n \lesssim 10^{10}$ cm^{-3}, and $\xi \sim 1$–100. Dissociative shocks produce

$$\xi_{shock} = 1.0 \frac{x_{-4}(H_2O) n_{07} v_{s7}}{\Delta v_5 \gamma_{-17}} , \quad (3.5)$$

as can be derived from equations (2.1), (3.1) and (3.4). Therefore, preshock densities within an order of magnitude of 3×10^7 cm^{-3} produce strong maser action. When n_0 is much less than this value, the plateau temperature (see eq. [3.3]) and the gas density are too low to excite the maser to high brightness temperatures. When n_0 is much greater than this value, the maser is either collisionally quenched or is so small ($d \propto n_0^{-1}$) that extremely high aspect ratios ($a > 100$) are required to provide saturation.

We have checked the analytic equations with several computer runs which varied the parameters of the standard case presented in Figure 2. For an identical model but with $b = 3$ we obtain $d \simeq 4 \times 10^{14}$ cm, $N_{plat} \simeq 10^{23}$ cm^{-2}, $T_{plat} = 400$ K, and $\xi_{shock} = 2$. These results agree with the scaling of the standard run using the analytic expressions. Stronger magnetic fields therefore produce maser spots with larger dimensions. The same effect is obtained by lowering the preshock density. However, n_0 cannot be lowered arbitrarily because the water abundance produced by the shock finally decreases. A model identical to the standard case but with $n_0 = 10^6$ cm^{-3} produced $d \simeq 6 \times 10^{13}$ cm, $N_{plat} \simeq 10^{22}$ cm^{-2}, $T_{plat} = 350$ K and $\xi_{shock} = 2.5 \times 10^{-2}$. These results are readily understood when we note that $x(H_2O)$ is only 3×10^{-5} for this run. Thus, an effective lower limit on the preshock density in our scheme is $n_0 \gtrsim 3 \times 10^6$ cm^{-3}.

Combining equations (2.1), (2.4), and (3.4), the isotropic luminosity of a shock-produced maser is

$$L_m = 2.7 \times 10^{-6} \lambda^{-1} \frac{\eta_{-2} q_{-11} x^2_{-4}(H_2O)}{\xi_{shock} \Delta v_5 \gamma^4_{-17}} b^4 a_1^3 f L_\odot . \quad (3.6)$$

The dependence on the properties of the ambiet medium enters only through ξ_{shock} (which determines also η_{-2} and q_{-11}) and b. Thus, for shocks that produce masers operating near peak performance the luminosity is very sensitive to the ambient field parameter b, which is proportional to the Alfvén velocity. We note, though, that $x_{-4}(H_2O)$ and γ_{-17} may also depend on ξ_{shock}, a dependence that will be explored in a future publication (Elitzur, Hollenbach and McKee, 1989). The inverse proportionality with ξ_{shock} follows because the column density of the shocked material is fixed by b (eq. [3.2]) so its ξ is directly related to the density (eq. [3.5]). Higher densities, or

$\xi_{\rm shock}$, correspond to smaller spot sizes (eq. [3.4]) and smaller dimensions lead to lower luminosities.

Finally, we note that slower ($v_s \lesssim 40$–50 km s^{-1}) *C*-shocks (see Draine 1980) may also produce similar physical conditions ($N_{\rm plat} \sim 10^{22}$ cm^{-2}, $n \sim 10^9$ cm^{-3}, $T \sim 10^3$ K, $T_{\rm gr} \sim 50$–100 K) if the preshock densities are of the order $n_0 \gtrsim 10^8$ cm^{-3}; this possibility will be explored in future work.

IV. SUMMARY AND DISCUSSION

Postshock gas provides the ideal environment for H_2O maser emission. For dissociative shocks, the appropriate physical conditions are produced for preshock densities $n_0 \sim 10^7$ cm^{-3} and shock velocities $v_s \gtrsim 50$ km s^{-1}. The results are quite robust with respect to other shock variables. The large velocity displacement of the individual spots is produced, at least in part, by the projection of the shock velocities along the line of sight. The high gas temperatures ($T \sim 400$ K) provide the necessary excitation energy. The chemistry in such gas naturally provides a high abundance ($\sim 10^{-4}$) and column density ($\sim 3 \times 10^{18}$ cm^{-2}) of H_2O. The observed width of the maser spot can be identified with the thickness of the postshock high-temperature H_2O layer ("plateau"). Such shocks provide the appropriate ξ (~ 1–10) that is required for the most efficient maser operation. Slower *C*-shocks may also provide similar conditions if $n_0 \gtrsim 10^8$ cm^{-3} and $v_s \gtrsim 10$ km s^{-1}.

In order to assess the validity of our model it is worth while to digress on the results of observations first. Although the range of brightness temperatures observed in W51, an average H_2O maser source, is $\sim 10^{11}$–10^{14} K, the majority of features have $T_b \simeq 10^{12}$ K (Genzel *et al.* 1981). This should therefore be regarded as the "typical" brightness temperature that models should attempt to explain. As seen from equation (2.3), our model would imply an aspect ratio of ~ 10 for the "typical" feature, with a range of $a \sim 5$–50 for all spots; the high end is required for only a couple of filaments. The situation in W49, the most powerful galactic maser, is similar (see below). The shock geometry is such that higher aspect ratios are expected when $\boldsymbol{v}_s$ is perpendicular to the line of sight; therefore, H_2O masers with low radial velocities should be brighter, as is observed. The variability time scale t_m for an H_2O maser is the time scale for velocity coherence to be maintained along the line of sight, or $t_m \gtrsim d/v_s \approx 1$ month, in agreement with observations (see Tarter and Welch 1986). If the filament is part of a sheet with a radius of curvature R, then there is a geometric limit on a: If d is the thickness of the sheet, then the maximum length of the filament is $(8Rd)^{1/2}$ and the maximum velocity coherence length is $(\Delta v/v_s)R$. As a result, the maximum aspect ratio is

$$a_{\rm max} = \min\,[(\Delta v/v_s)(R/d), (8R/d)^{1/2}]\ . \qquad (4.1)$$

For example, if $\Delta v/v_s = 2 \times 10^{-2}$, an aspect ratio of 50 can be achieved in principle if R exceeds $2.5 \times 10^{16} d_{13}$ cm, comparable with the observed sizes of clusters of spots. The filaments required by our model are not a pecularity of maser sources. Recent CO mapping by Bally *et al.* (1987) and Bally and Yusef-Zadeh (1989) of the giant molecular cloud in Orion and the Galactic center show filamentary structure, with aspect ratios as large as 40.

Exceptional brightness temperatures, much greater than 10^{14} K, appear to have been recorded in only two maser bursts, one of which occurred in W49 in 1971 (Burke *et al.* 1973) and one in Orion in 1979 (Abraham *et al.* 1981; Matveenko, Moran, and Genzel 1982). These transient brightness temperatures are associated with unusually small dimensions and linewidths (Matveenko 1986; Garay, Moran, and Haschick 1989). These appear to be unique events which should be dealt with separately, and we reserve their discussion to a future publication.

The most luminous maser in the Galaxy is W49N, with a maximum luminosity from one spot of $\sim 0.08\ L_\odot$ corresponding to an observed flux density of 4,495 Jy in a line width of 3.6 km s^{-1} (Walker *et al.* 1982) and an observed size $\gtrsim 10^{14}$ cm (Walker 1984). Such a luminosity results from $a = 37$, using equation (2.5) with $f = 1$ and the observed parameters; the corresponding brightness temperature is 7.6×10^{13} K. The observed spot size can be obtained, as noted in § III, with a preshock density of 10^7 cm^{-3} and $b \simeq 1.5$. The next most luminous spot has $L_m = 0.06\ L_\odot$. It displays a higher brightness of 9515 Jy in a smaller line width of 1.3 km s^{-1} and would require a slightly larger $a = 48$, corresponding to $T_b = 1.6 \times 10^{14}$ K. It is important to note that out of the 386 maser features in W49N listed by Walker *et al.* the majority have brightness of ~ 100 Jy or less and only 15 features are brighter than 1000 Jy. The high-luminosity spots, which require a combination of large sizes with high aspect ratios, correspond to the tail end of the distribution. Their relative rarity may be due to the large fields required and to the unlikelihood of such large velocity coherence path lengths.

It is many times assumed, implicitly or explicitly, that H_2O maser emission is correlated with density such that the more powerful sources have higher densities. This expectation is not borne out by our model even though the pumping is by collisions. For operation near peak performance, that is $\xi \simeq 24$, the brightness temperature is correlated only with aspect ratio (eq. [2.3]) while the luminosity depends also on the line width and the filamentary diameter (eq. [2.5]). Neither the brightness nor the luminosity then depend directly on density (provided, of course, that it falls in the range $\sim 10^8$–10^{10} cm^{-3} so that the various constraints set by the model are met.) In fact, the more luminous spots are probably characterized by large diameters which, at fixed ξ and b, correspond to *smaller* densities. In all likelihood, a high maser luminosity is indicative of a relatively large preshock magnetic field (eq. [3.6]). We must caution, however, against the expectation of tight correlations. As seen from Figure 1, there is a rather large range of ξ where the maser operation is close to maximum efficiency.

There are several testable predictions of our model.

i) *Other Maser Lines*

As was the case in previous calculations (de Jong 1973; Cooke and Elitzur 1985), a large number of H_2O lines are inverted. The $6_{16} \rightarrow 5_{23}$ maser stands out among those as the transition with the longest wavelength and the one whose inversion persists to the largest diameters. Bright 22 GHz filaments can therefore emit other maser lines only from their outer skin layers. The $4_{14} \rightarrow 3_{21}$ maser at 789 μm, which may have been detected in Orion (Phillips, Kwan, and Huggins 1979), reaches peak brightness at $\xi = 0.1$ with $q_{-11} = 0.9$ and $\eta_{-2} = 1.6$. Thus, from equation (2.2) the peak brightness temperature of this maser is

$$T_{b,\rm peak}(789\ \mu{\rm m}) \simeq 1.2 \times 10^8 a_1^3 f\ {\rm K}\ . \qquad (4.2)$$

This maser is quenched when $\xi \gtrsim 0.3$ and filaments that are strong emitters of the 22 GHz line cannot reach saturated operation in the 789 μm maser for reasonable aspect ratios. In

general, therefore, the two lines cannot be emitted from the same maser feature. From equation (3.6) the isotropic luminosity of a 789 μm maser operating near its peak brightness temperature is

$$L_m(789\ \mu\text{m}) = 4.9 \times 10^{-4}\ \frac{x^2_{-4}(H_2O)}{\Delta v_5\, \gamma^4_{-17}}\ b^4 a_1^3 f\, L_\odot\ . \quad (4.3)$$

Because of the lower value of ξ, observable maser operation requires shocks running into relatively low ambient densities ($n_0 \sim 10^6$ cm^{-3}; see eq. [3.5]). This also ensures that the corresponding diameters are sufficiently large that saturation can be obtained at reasonable aspect ratios. However, $x_{-4}(H_2O)$ is reduced for low-density shocks (§ III), a point that we plan to address in a more complete manner in the future. The shocks must also produce the temperature plateau with the appropriate column density. Combining equations (3.3) and (3.5) we find

$$T_{\text{plat}} \simeq 400\left(\frac{\xi_{\text{shock}}\, \gamma_{-17}}{x_{-4}(H_2O)}\right)^{2/9}\ \text{K}\ , \quad (4.4)$$

provided the preshock density exceeds $\sim 10^5$ cm^{-3} so that the temperature plateau can develop. Thus, shocks with $\xi = 0.1$ can still produce $T_{\text{plat}} \simeq 240$ K, enough to populate the 4_{14} state which lies only 225 cm^{-1} above the ground state.

The situation for other maser transitions is similar. The $8_{27} \rightarrow 7_{34}$ line at 231 μm is the only other maser that can maintain its inversion up to $\xi \simeq 0.3$. Peak brightness temperature is obtained at $\xi = 0.16$, where $q_{-11} = 0.08$ and $\eta_{-2} = 6.8$. Thus, most of the properties of this maser are similar to those of the 789 μm maser, the major exception being the higher temperatures required to populate its levels. The other maser transitions listed by Cooke and Elitzur are all quenched at lower values of ξ.

ii) *Shock Luminosity*

Most of the emission from the shock is reprocessed into far-infrared continuum by dust. If the area of the shock front associated with a single maser feature is $\alpha(ad)^2$, where we expect $\alpha \gtrsim 1$, then each shock radiates $L_s = 0.03 n_{07}\, v_{s7}^3 \alpha (a_1 d_{13})^2\ L_\odot$. We see only a small fraction $2\Omega_m/4\pi = 3/(14fa^2)$ of the masers in a given region, however, where the factor 2 allows for maser emission from both ends of the filament and where the beaming angle in the Goldreich and Keeley (1972) model is $3\pi/(7a^2)$. For a region in which we observe $\mathcal{N}_m$ masers, the expected value of the total shock luminosity is then

$$L_t = 143 n_{07}\, v_{s7}^3\, \alpha a_1^4 (\mathcal{N}_m/10) d_{13}^2\, f\, L_\odot\ , \quad (4.5)$$

assuming that each maser spot corresponds to a shock. This is a lower limit to the mechanical luminosity of the source driving the outflow producing the masers. A few percent of this luminosity appears in molecular (mostly OH and H_2O) emission lines from the postshock gas.

iii) *Magnetic Fields*

Unless the upstream magnetic field is extremely weak ($b \lesssim 0.1$) the magnetic field dominates the pressure in the masing region (see HM), and

$$B_{\text{maser}} = 0.24(n_{07}\, v_{s7}^2)^{1/2}\ \text{G} = 0.28(b n_9\, v_{s7})^{1/2}\ \text{G}\ . \quad (4.6)$$

For the conditions we have inferred for galactic water masers, the factor in parentheses is of order unity. This result is in reasonable agreement with the recent measurements by Fiebig and Gusten (1989) of H_2O Zeeman splitting. They find that one hyperfine component dominates the lines they observed, although the reason for this is not clear. The inferred magnetic field is ~ 0.05 G (0.08 G) if this is the $F = 7$–6 ($F = 6$–5) component, which are the two strongest components in LTE. (If the observed component were the $F = 5$–4 transition, the inferred field would be 0.7 G.) The sharp upper boundary on $B_\parallel$ displayed by these observations may find a natural explanation in our model because velocity coherence is more likely to occur along the field lines (motions across field lines tend to be suppressed). The pointing of the filaments may therefore introduce a kinematic correlation between maser luminosity and measured $B_\parallel$. Note also that these magnetic fields are large enough to account for the linear polarization observed in many water masers (Deguchi and Watson 1986).

An interesting result is obtained by combining equations (2.1) and (3.4):

$$b = 0.77\gamma_{-17}\left(\frac{\xi\, \Delta v_5\, d_{13}}{x_{-4}(H_2O)}\right)^{1/2}\ . \quad (4.7)$$

which corresponds to a *preshock* magnetic field of

$$B_0 = 2.4\ \frac{\xi}{x_{-4}(H_2O)}\left(\frac{\gamma^3_{-17}\, \Delta v_5\, d_{13}}{v_{s7}}\right)^{1/2}\ \text{mG}\ . \quad (4.8)$$

Bigger maser spots are therefore associated with stronger preshock magnetic fields, all other parameters being equal. Thus, although similar brightness temperatures can be produced over a rather large range of dimensions, as evident from Figure 1, it seems likely that the most luminous maser spots are indeed the result of strong magnetic fields in the unshocked gas, which lead to large dimensions. This is also evident from equation (3.6).

Finally, we comment on the relation between the magnetic field and the density in the masing region. Magnetic fields in self-gravitating clouds are predicted to scale with density approximately as $n^{1/2}$ (Mouschovias 1976; Mestel 1985), corresponding to a constant Alfvén velocity, and this is in accord with observations (Myers and Goodman 1988). As shown by relation (4.6), shock models predict the same correlation, but with a greater coefficient:

$$b_{\text{maser}} \equiv \left(\frac{B_{\text{maser}}}{1\ \mu\text{G}}\right) n^{-1/2} = \left(\frac{n}{n_0}\right)^{1/2} b = 8.8(b v_{s7})^{1/2}\ . \quad (4.9)$$

For J-shocks, the density in the masing region, which is behind the shock, is much greater than n_0 and hence $b_{\text{maser}} > b$. For C-shocks, the magnetic field is compressed before the neutral gas (Draine 1980), so that b_{maser} is generally larger than b in this case as well.

iv) *Extragalactic Masers*

Water masers with isotropic luminosities of up to $\sim 350\ L_\odot$ have been observed in the nuclei of external galaxies (Dos Santos and Lepine 1979; Claussen, Heiligman, and Lo 1984; Claussen and Lo 1986). The maser activity is confined to within a few parsecs at the center of the galaxy, which evidently contains many maser features. Such a high, concentrated maser activity does not exist in our own Galaxy. The question, then, is whether the single maser spots are different from those in our Galaxy and whether some special, esoteric pumping scheme has to be invoked to explain them.

Unfortunately, extragalactic masers cannot be resolved on the linear scales ($\sim 10^{13}$–10^{14} cm) that typify Galactic maser

spots and which are implied by our model. This is a point of concern because spectral blending can severely distort the underlying structure. For example, although the velocity peaks of the three brightest maser features in W49N fall within a velocity interval of only 0.7 km s^{-1}, their positions are very different (Walker *et al.* 1982). A single-dish measurement would therefore lump these features together, even though they are unrelated. With these caveats in mind, it is important to ask what is the maximum single-spot luminosity that can be produced by our model. Using the extreme, although still reasonable, parameters $a = 70$, $d = 5 \times 10^{14}$ cm, and $\Delta v = 10$ km s^{-1}, equation (2.5) yields $L_m = 40\ L_\odot$ for a single maser spot; the minimum radius of curvature implied is 3×10^{17} cm (eq. [4.1]), consistent with the observed size of the nuclear region. Such a high single-spot luminosity appears sufficient to explain the observations. The most stringent constraints seem to follow from the variability on a time scale of $\sim 5 \times 10^6$ s of a spectral feature in NGC 4258 with $L_m \simeq 40\ L_\odot$ and $\Delta v_5 \simeq 10$ (Claussen *et al.* 1984). With a shock velocity of 200 km s^{-1} this corresponds to $d = 10^{14}$ cm, somewhat smaller than in our model. Note, however, that if more than one filament is observed from a given shock, then they can vary coherently and the discrepancy is reduced. Indeed, recent observations show that the feature has split into two narrower components with smaller luminosities (Claussen 1988).

It thus seems that our model is capable of explaining the single maser spots of extragalactic masers as similar in nature to those in our own galaxy, although covering a larger range of luminosities; Ho *et al.* (1987) have recently reached the same conclusion, based on their observations of NGC 253 and M51. From equation (4.8) it follows that the preshock magnetic field is $B_0 \sim 50\xi$ mG for the parameters we inferred for the most luminous spots; since $\xi \gtrsim 1$ for efficient masing, this implies $B_0 \gtrsim 50$ mG. Strong magnetic fields of this magnitude have been inferred at the Galactic center (Aitken *et al.* 1986; Werner *et al.* 1988). Furthermore, this estimate is consistent with the upper limit of 300 mG found by Fiebig and Gusten (1989) for NGC 3079, the brightest extragalactic source. Note that if the oxygen abundance is higher than solar in the galactic nucleus, then the inferred field strength is reduced somewhat.

In conclusion, our calculations show that H_2O maser emission results naturally from the physical conditions that occur behind shock fronts. With the possible exception of two burst sources, unconventional pumping schemes are not called for. The possibility of maser emission from other sources will be explored in a forthcoming publication, which will also present a more detailed study of the pump conditions including other possible pump mechanisms.

We would like to thank S. Green for his effort in calculating the H_2O collision rates and his permission to use them prior to publication; J. Bally for a very helpful discussion that led to the detailed study of filamentary masers; M. Claussen and K. Y. Lo for clarifying issues concerning extragalactic masers; and C. Gwinn for discussions of his recent observations of W49. Part of this work was performed while M. E. was a visitor at NASA Goddard Space Flight Center, supported by an NAS/NRC associate fellowship. We also acknowledge the support of NSF through grants AST 83-04895, AST 86-15177, and AST 87-16936, and NASA RTOPS 188-41-53 and 188-48-52.

REFERENCES

Abraham, Z., *et al.* 1981, *Astr. Ap.*, **100**, L10.
Alcock, C., and Ross, R. R. 1985, *Ap. J.*, **290**, 433.
Aitken, D. K., *et al.* 1986, *M.N.R.A.S.*, **218**, 363.
Bally, J., *et al.* 1987, *Ap. J. (Letters)*, **312**, L45.
Bally, J., and Yusef-Zadeh, F. 1989, *Ap. J.*, **336**, 173.
Burke, B. F., *et al.* 1973, *Izv. Vyssh. Uchebn. Zaved., Radiofiz.*, **16**, 799.
Capriotti, E. R. 1965, *Ap. J.*, **142**, 1101.
Chernoff, D. F., Hollenbach, D. J., and McKee, C. F. 1982, *Ap. J. (Letters)*, **259**, L97.
Claussen, M. J. 1988, private communication.
Claussen, M. J., Heiligman, G. M., and Lo, K. Y. 1984, *Nature*, **310**, 298.
Claussen, M. J., and Lo, K. Y. 1986, *Ap. J.*, **308**, 592.
Comsa, G., and David, R. 1985, *Surface Sci. Rept.*, **5**, 145.
Cooke, B., and Elitzur, M. 1985, *Ap. J.*, **295**, 175.
Deguchi, S., and Watson, W. D. 1986, *Ap. J.*, **302**, 750.
de Jong, T. 1973, *Astr. Ap.*, **26**, 297.
Dos Santos, P. M., and Lepine, J. R. D. 1979, *Nature*, **278**, 34.
Draine, B. T. 1980, *Ap. J.*, **241**, 1021.
Duley, W. W., and Williams, D. A. 1986, *M.N.R.A.S.*, **223**, 177.
Elitzur, M. 1979, *Ap. J.*, **229**, 560.
———. 1982, *Rev. Mod. Phys.*, **54**, 1225.
———. 1989, in preparation.
Elitzur, M., Hollenbach, D. J., and McKee, C. F. 1989, in preparation.
Elitzur, M., McKee, C. F., and Hollenbach, D. J. 1989, in preparation.
Fiebig, D., and Gusten, R. 1989, *Astr. Ap. Letters*, **214**, 333.
Garay, G., Moran, J. M., and Haschick, A. D. 1989, *Ap. J.*, **338**, 244.
Genzel, R. 1986, in *Masers, Molecules, and Mass Outflows in Star Forming Regions*, ed. A. D. Haschick (Westford, MA: Haystack Observatory), p. 233.
Genzel, R., *et al.* 1979, *Astr. Ap.*, **78**, 239.
———. 1981, *Ap. J.*, **247**, 1039.
Goldreich, P., and Keeley, D. A. 1972, *Ap. J.*, **174**, 517.
Green, S. 1980, *Ap. J. Suppl.*, **42**, 103.
Ho, P. T. P., Martin, R. N., Henkel, C., and Turner, J. L. 1987, *Ap. J.*, **320**, 663.
Hollenbach, D. J., and McKee, C. F. 1979, *Ap. J. Suppl.*, **41**, 555 (HM).
———. 1989, *Ap. J.*, in press.
Hollenbach, D. J., McKee, C. F., and Chernoff, D. 1987, in *Star Forming Regions*, ed. M. Peimbert and J. Jugaku (Dordrecht: Reidel), p. 334.
Hollenbach, D. J., and Salpeter, E. E. 1971, *Ap. J.*, **163**, 155.
Hunter, D. A., and Watson, W. D. 1978, *Ap. J.*, **226**, 477.
Kylafis, N. D., and Norman, C. 1986, *Ap. J. (Letters)*, **300**, L73.
Lin, T. H., and Somorjai, G. A. 1985, *J. Chem. Phys.*, **89**, 135.
Lucas, R. 1980, *Ast. Ap.*, **84**, 36.
Matveenko, L. I. 1986, *Soviet Astr.*, **30**, 589.
Matveenko, L. I., Moran, J. M., and Genzel, R. 1982, *Soviet Astr. Letters*, **8**, 382.
Mestel, L. 1985, in *Protostars and Planets II*, ed. D. Black and M. Matthews (Tucson: University of Arizona Press), p. 320.
McKee, C. F., Hollenbach, D. J., Seab, C. G., and Tielens, A. G. G. M. 1987, *Ap. J.*, **318**, 674.
Mouschovias, T. 1976, *Ap. J.*, **207**, 141.
Myers, P. C., and Goodman, A. A. 1988, *Ap. J. Letters*, **326**, L27.
Neufeld, D. A., and Melnick, G. J. 1987, *Ap. J.*, **322**, 266.
Palma, A., Green, S., DeFrees, D. J., and McLean, A. D. 1988, *Ap. J. Suppl.*, **68**, 287.
Phillips, T. G., Kwan, J., and Huggins, P. J. 1979, in *Interstellar Molecules*, ed. B. H. Andrew (Dordrecht: Reidel), p. 21.
Shutte, A., *et al.* 1976, *J. Chem. Phys.*, **64**, 4135.
Strelnitskij, V. S. 1978, *Soviet Astr.*, **21**, 381.
———. 1980, *Astr. Zh., Pis'ma* **6**, 354.
———. 1984, *M.N.R.A.S.*, **207**, 339.
Tarter, J. C., and Welch, W. J. 1986, *Ap. J.*, **305**, 467.
Walker, R. C. 1984, *Ap. J.*, **280**, 618.
Walker, R. C., Matsakis, D. N., and Garcia-Barreto, J. A. 1982, *Ap. J.*, **255**, 128.
Werner, M., Davidson, J. A., Morris, M., Novak, G., Platt, S. R., and Hildebrand, R. H. 1988, *Ap. J.*, **333**, 729.

M. ELITZUR: Department of Physics and Astronomy, University of Kentucky, Lexington, KY 40506-0055

D. J. HOLLENBACH: NASA-Ames Research Center, MS 245-6, Moffett Field, CA 94035

C. F. MCKEE: Astronomy Department, Campbell Hall, University of California, Berkeley, CA 94720